



GIS-based gully erosion susceptibility mapping: a comparison among three data-driven models and AHP knowledge-based technique

Alireza Arabameri¹ · Khalil Rezaei² · Hamid Reza Pourghasemi³ · Saro Lee⁴ · Mojtaba Yamani⁵

Received: 28 February 2018 / Accepted: 3 September 2018 / Published online: 10 September 2018
© Springer-Verlag GmbH Germany, part of Springer Nature 2018

Abstract

Toroud Watershed in Semnan Province, Iran is a prone area to gully erosion that causes to soil loss and land degradation. To consider the gully erosion, a comprehensive map of gully erosion susceptibility is required as useful tool for decreasing losses of soil. The purpose of this research is to generate a reliable gully erosion susceptibility map (GESM) using GIS-based models including frequency ratio (FR), weights-of-evidence (WofE), index of entropy (IOE), and their comparison to an expert knowledge-based technique, namely, Analytic Hierarchy Process (AHP). At first, 80 gully locations were identified by extensive field surveys and Google Earth images. Then, 56 (70%) gully locations were randomly selected for modeling process, and the remaining 26 (30%) gully locations were used for validation of four models. For considering geo-environmental factors, VIF and tolerance indices are used and among 18 factors, 13 factors including elevation, slope degree, slope aspect, plan curvature, distance from river, drainage density, distance from road, lithology, land use/land cover, topography wetness index (TWI), stream power index (SPI), normalized difference vegetation index (NDVI), and slope–length (LS) were selected for modeling aims. After preparing GESMs through the mentioned models, final maps divided into five classes including very low, low, moderate, high, and very high susceptibility. The receiver operating characteristic (ROC) curve and the seed cell area index (SCAI) as two validation techniques applied for assessment of the built models. The results showed that the AUC (area under the curve) in training data are 0.973 (97.3%), 0.912 (91.2%), 0.939 (93.9%), and 0.926 (92.6%) for AHP, FR, IOE, and WofE models, respectively. In contrast, the prediction rates (validating data) were 0.954 (95.4%), 0.917 (91.7%), 0.925 (92.5%), and 0.921 (92.1%) for above models, respectively. Results of AUC indicated that four model have excellent accuracy in prediction of prone areas to gully erosion. In addition, the SCAI values showed that the produced maps are generally reasonable, because the high and very high susceptibility classes had very low SCAI values. The results of this research can be used in soil conservation plans in the study area.

Keywords Soil conservation · Spatial modeling · Validation · SCAI · Toroud watershed

✉ Hamid Reza Pourghasemi
hamidreza.pourghasemi@yahoo.com;
hr.pourghasemi@shirazu.ac.ir

- ¹ Physical Geography (Geomorphology), Tarbiat Modares University, Tehran, Iran
- ² Faculty of Earth Sciences, Kharazmi University, Tehran, Iran
- ³ Department of Natural Resources and Environmental Engineering, College of Agriculture, Shiraz University, Shiraz, Iran
- ⁴ Geological Research Division, Korea Institute of Geoscience and Mineral Resources (KIGAM), 124, Gwahak-ro Yuseong-gu, Daejeon 34132, South Korea
- ⁵ Physical Geography (Geomorphology), Tehran University, Tehran, Iran

Introduction

The Earth system has been impacted by mankind abuse of resources, lack of management of land uses and planning, and climate changes that imposed changes to the natural environment such as the water, soil, and carbon or nitrogen cycles, which is resulting in land degradation (Keesstra et al. 2018). Thus, the United Nation has defined the Sustainable Development Goals (SDGs) (Griggs et al. 2013). Many of the defined goals have a strong relevance to water and soil management. Soil is one of the most important components of hydrological, biological, and geological cycles and, therefore, is in a state of permanent change and evolution (Kirchhoff et al. 2017). European Commission defined

seven functions for soil including: (1) biomass production including forestry and agriculture; (2) storing, filtering, and transforming nutrients, substances, and water; (3) biodiversity pool such as habitats, species, and genes; (4) physical and cultural environment for humans and human activities; (5) source of raw material; (6) acting as carbon pool; and (7) archive of geological and archaeological heritage (EC, 2006). In the twenty-first century, soil protection depends not only on political decisions in the rules and regulations, but also on decisions and actions of land planners, foresters, and farmers (Cerdà et al. 2017a, b). Soil erosion is a universally threat to environment that leads to a various range of problems, such as land degradation in agriculture lands, soil fertility reduction, and sediment deposition in reservoirs, that must be solved by means of nature-based strategies (Cerdà et al. 2016; Keesstra et al. 2016; Mekonnen et al. 2017). High erosion rates in underdeveloped countries are mainly due to lack of vegetation cover, excessive grazing, deforestation, and intense plowing (Ligonja and Shrestha 2015), while in the developing countries is due to the heavy machinery (Cerdà et al. 2009). Intense erosion rates result in the loss of fertile soil and also change on the biological, hydrological, and geochemical cycles (Cerdà et al. 2015). Gully erosion is one of the most devastating forms of soil erosion that causes different types of damage to natural resources, agriculture, and infrastructures (Rahmati et al. 2016). A gully is defined as a profound channel created by concentrated flow of water, removing surface soil, and parent material, that is really big to wipe out by normal tillage operations (USDA-SCS 1966). When the geomorphologic threshold exceeds due to increase in flow water erosivity or sediment erodibility, gully erosion is occurred. In general, prediction of gully erosion is difficult and requires monitoring and mapping (Rahmati et al. 2017). Preparation of gully erosion susceptibility map (GESM) is necessary for better realization of the gully erosion mechanism and identifying areas that are prone to erosion. For this target, gully inventory map (GIM) and GEFs are required. Meanwhile, the results of a GESM strongly depend on the model hypothesis, parameter values, and parameter estimation methods. From the point of view of reducing the occurrence of gully erosion and sustainable development, there are many models for establishing a statistical relationship among GEFs and GIM and subsequently identifying sensitive areas to gully erosion. Among these are the following data-driven and knowledge-based models: logistic regression (Conoscenti et al. 2014; Kornejady et al. 2015), weights-of-evidence (Dube et al. 2014; Rahmati et al. 2016), frequency ratio (Rahmati et al. 2016), conditional probability (Rahmati et al. 2017); AHP (Svoray et al. 2012), maximum entropy (Pourghasemi et al. 2017; Kornejady et al. 2017), and information value (Conforti et al. 2011). In addition, computational intelligence methods including classification and regression trees

(Märker et al. 2011), multivariate adaptive regression splines (Gómez-Gutiérrez et al. 2015), random forest (Kuhnert et al. 2010), artificial neural network (Pourghasemi et al. 2017), and support vector machine (Pourghasemi et al. 2017) were applied for preparing GESM in different countries.

In the study area, due to dry climatic conditions, extreme rainfall, favorable erosion geology, overgrazing, and vegetation destruction, gully erosion is the most important cause of soil degradation and soil loss. Therefore, gully erosion each year imposes damages on the inhabitants and agricultural lands. Despite the fact that gully erosion is one of the environmental problems in the Toroud Watershed, so far, no studies have been carried out in this area to assess and prepare a gully erosion susceptibility map for it. The main purpose of this research is identification of prone areas to gully erosion and gully erosion susceptibility mapping using data-driven and knowledge-based techniques in Toroud Watershed, Iran.

Materials and methods

Study area

The Toroud Watershed with area of 416 km² is situated in Semnan Province, Iran. This area is located between 35°25'36" and 35°37'9" north latitudes, and 54°49'55" and 55°11'30" east longitudes (Fig. 1). According to the climatic classification in Iran (IDWRM 2013), the study area is classified as arid zone (mean annual rainfall of 85 mm). The absolute elevation in the study area ranges from about 759 to 1923 m, with a mean elevation of 1037 m a.s.l. It receives approximately 80% of its annual rainfall from November to April (WRCS 2015). In winter, the temperature ranges from −5 to 12.7 °C. The main LC in the study area is irrigation agriculture, salt pan, and range lands. Most gullies in the study area are located on the southern parts due to erosion-sensitive formations and human activities such as agriculture, overgrazing, and development of roads. Eight photographs of the gullies identified in the study area are shown in Fig. 2.

Methodology

The methodological work flow used in the current study is presented in Fig. 3. Therefore, the steps of this research are as follows: (1) preparation of GIM; (2) selection of GEFs using VIF and tolerance indices; (3) preparation of gully erosion susceptibility maps using data-driven techniques (FR, IOE, and WofE), and their comparison to knowledge-based model, namely, AHP; (4) validation of models using ROC and SCAI indicators; and (5) selection of the best model in the study area.

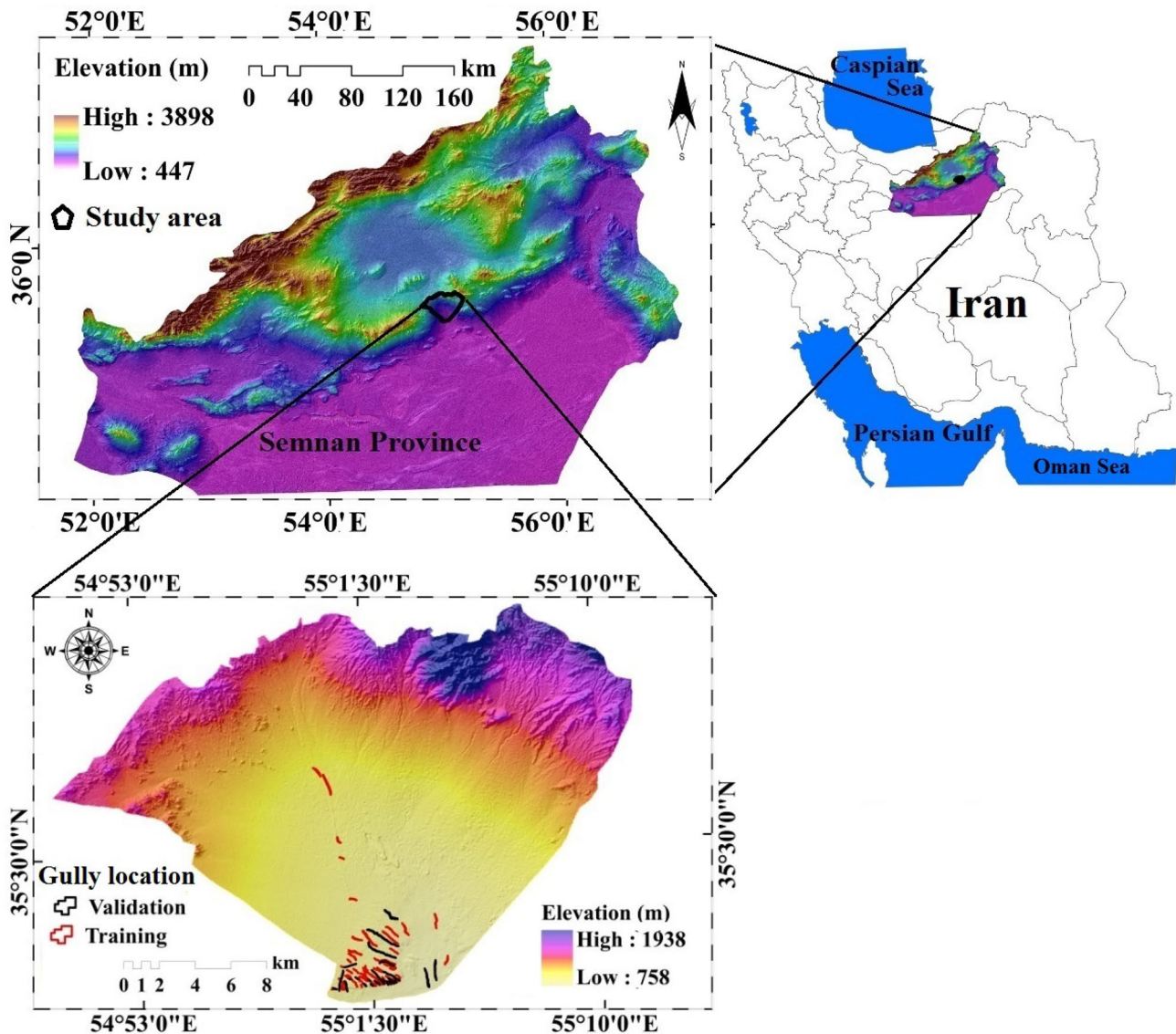


Fig. 1 Study area

Data preparation

Gully inventory map (GIM)

The detailed and accurate GIM was prepared using extensive field surveys with a GPS (Global Positioning System) device and Google Earth imagery digitization. Identified gullies in the study area are either V-shaped or U-shaped. In total, 80 gullies were identified summing an area of about 49.23 ha and include 53 V-shaped and 27 U-shaped gullies. Maximum and minimum depth and width of the identified gullies in the study area are 13.5 and 1.5 and 21 and 2.10, respectively. Among all the 80 identified gully locations, 70% (56 gully locations) were randomly selected for modeling, while the remaining 30% (24 gully location)

were employed for validation of models. In the next step, gullies in the polygon format were converted to point format and were used for modeling and validation aims. The locations of training and validating gullies are shown in Fig. 1.

Gullies in the study area are mainly created in low plains and slopes with high drainage density. The most important reason for occurring piping and gully in the study area is severe and flood rainfall, the existence of gypsum and salt minerals due to high evaporation, and the lack of vegetation and organic matter. Therefore, it can be admitted that superficial flows and the phenomenon of piping are the dominant processes of gully formation in the study area.



Fig. 2 Field photographs of some gullies identified in the study area

Gully erosion-conditioning factors

According to literature review (Conforti et al. 2011; Conoscenti et al. 2013; Zakerinejad and Maerker 2015; Rahmati et al. 2016, 2017; Pourghasemi et al. 2017; Zabihi et al. 2018), data availability, and field surveys, 18 effective factors were identified for considering gully erosion in the study area. After multi-collinearity analysis, 13 GEFs including elevation, slope degree, slope aspect, plan curvature, distance from river, drainage density, distance from road, lithology, LC, TWI, SPI, NDVI, and slope–length (LS) selected for modeling process (Fig. 4a–m).

Topographic factors are one of the most important geomorphological parameters that influence soil erosion (Achour et al. 2017; Rahmati et al. 2017). Topographic features such as elevation affect vegetation type and rainfall

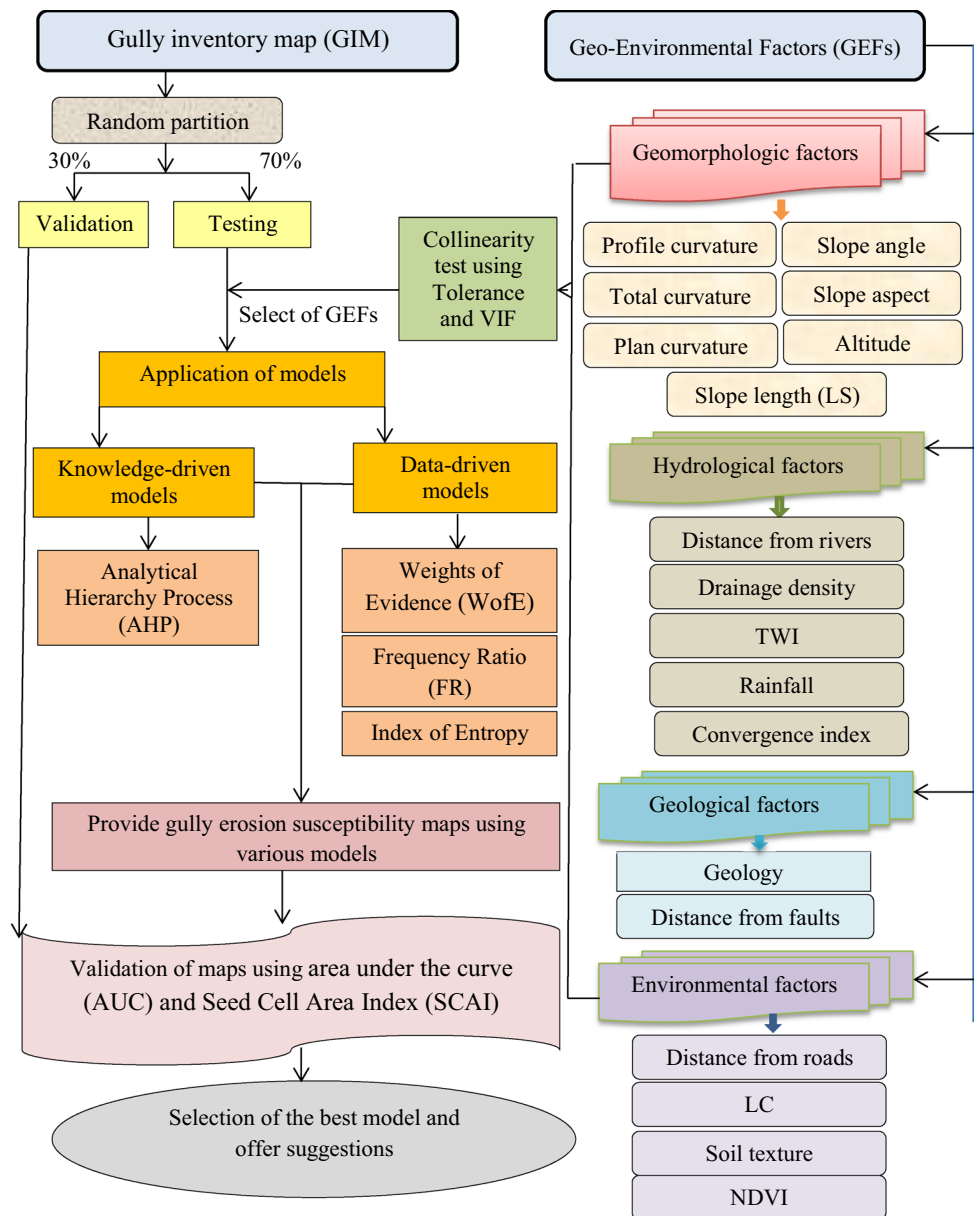
characteristics and, thus, can control the gully erosion process (Gómez-Gutiérrez et al. 2015).

In this research, to provide a digital elevation model, InSAR (Interferometric Synthetic Aperture Radar) technique and ALOS PALSAR data were used. For preparing DEM using InSAR, there are two phases including measurement phase and the conversion of measurement phase to height (Zhou et al. 2005). InSAR data-processing procedure is shown in Fig. 5.

Elevation obtained from the ALOS PALSAR Digital Elevation Model with a spatial resolution of $12.5 \text{ m} \times 12.5 \text{ m}$ and was divided into five categories (Rahmati et al. 2016): $<916 \text{ m}$, $916\text{--}1065 \text{ m}$, $1065\text{--}1229 \text{ m}$, $1229\text{--}1473 \text{ m}$, and $>1473 \text{ m}$.

Slope factor is appropriate for the accumulation of flow surface and gully erosion (Rahmati et al. 2016). The slope

Fig. 3 Methodological work flow used in this study



angle map of the study area was obtained from the ALOS PALSAR-DEM and was divided into six categories (Conforti et al. 2011): $<5^\circ$, $5^\circ-10^\circ$, $10^\circ-15^\circ$, $15^\circ-20^\circ$, $20^\circ-30^\circ$, and $>30^\circ$.

Slope aspect has an important effect on vegetation type, so the control duration of sunlight, moisture, evaporation and transpiration, and the distribution of vegetation on the slopes, and indirectly affect the erosion process (Jaafari et al. 2014). The slope aspect map was also prepared from ALOS PALSAR-DEM under nine directional classes (Rahmati et al. 2016): flat (-1°), north ($337.5^\circ-360^\circ$, $0^\circ-22.5^\circ$), northeast ($22.5^\circ-67.5^\circ$), east ($67.5^\circ-112.5^\circ$), southeast ($112.5^\circ-157.5^\circ$), south ($157.5^\circ-202.5^\circ$), southwest ($202.5^\circ-247.5^\circ$), west ($247.5^\circ-292.5^\circ$), and northwest ($292.5^\circ-337.5^\circ$).

Plan curvature is considered as the earth surface geometry and characterizes slope changes (Nefeslioglu et al. 2008). Plan curvature is effect on convergence or divergence of flow water during downhill flow (Yilmaz et al. 2012). Plan curvature was extracted from the ALOS PALSAR-DEM using ArcGIS 10.5 and classified into three categories including concave, flat, and convex.

In many cases, gullies are associated with stream network (Conoscenti et al. 2014). Using the quantile classification (Jiuchun et al. 2017), five different buffer zones are created within the study area to determine the effect of streams on gullies including: 0–100 m, 100–200 m, 200–300 m, 300–400 m, and >400 m.

The drainage pattern of an area is affected by several factors such as the nature and structure of geological

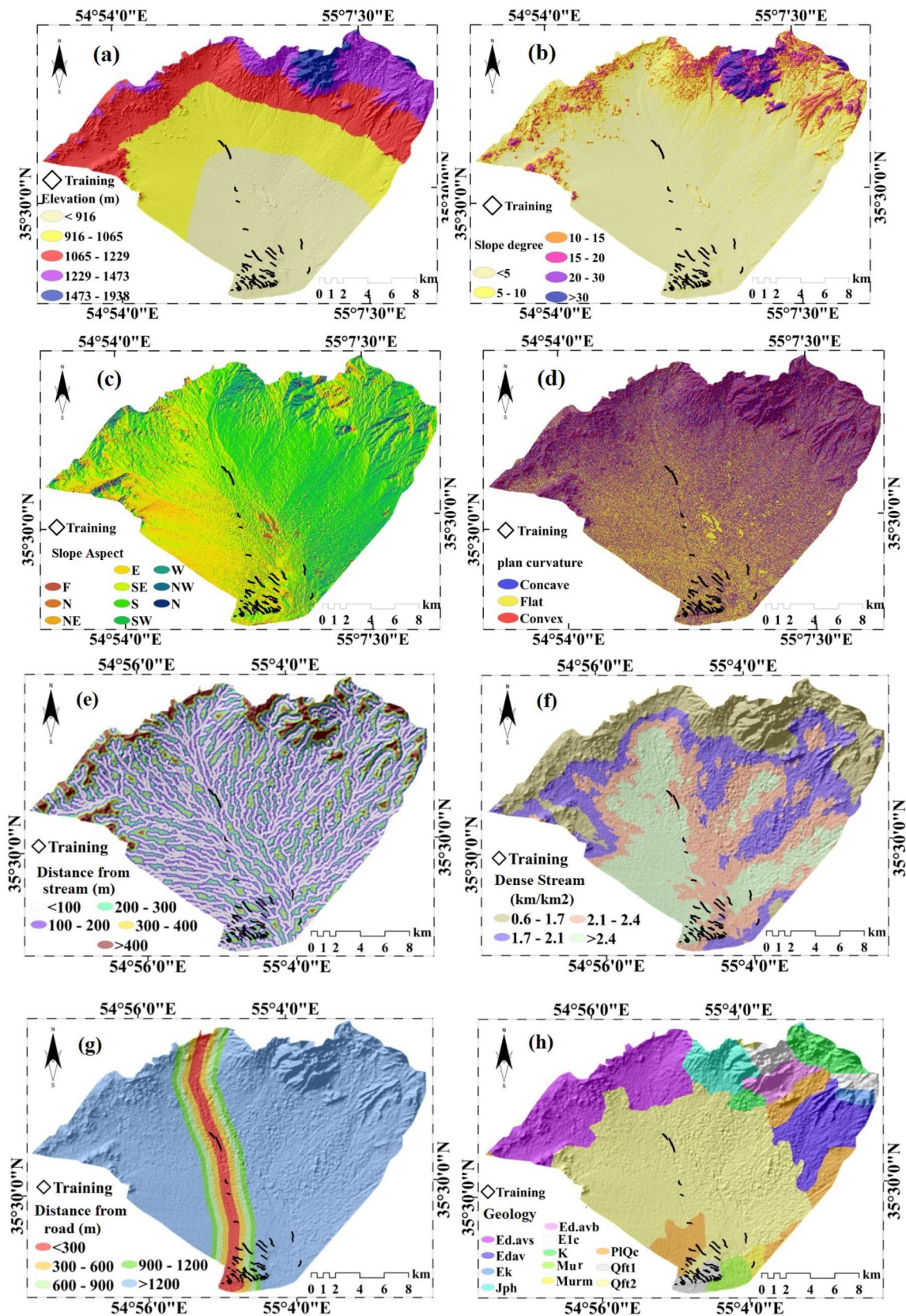


Fig. 4 Gully geo-environmental factors (GEFs). **a** Elevation, **b** slope degree, **c** slope aspect, **d** plan curvature, **e** distance from river, **f** drainage density, **g** distance from road, **h** lithology, **i** land cover, **j** topogra-

phy wetness index (TWI), **k** stream power index (SPI), **l** normalized difference vegetation Index (NDVI), and **m** slope-length (LS)

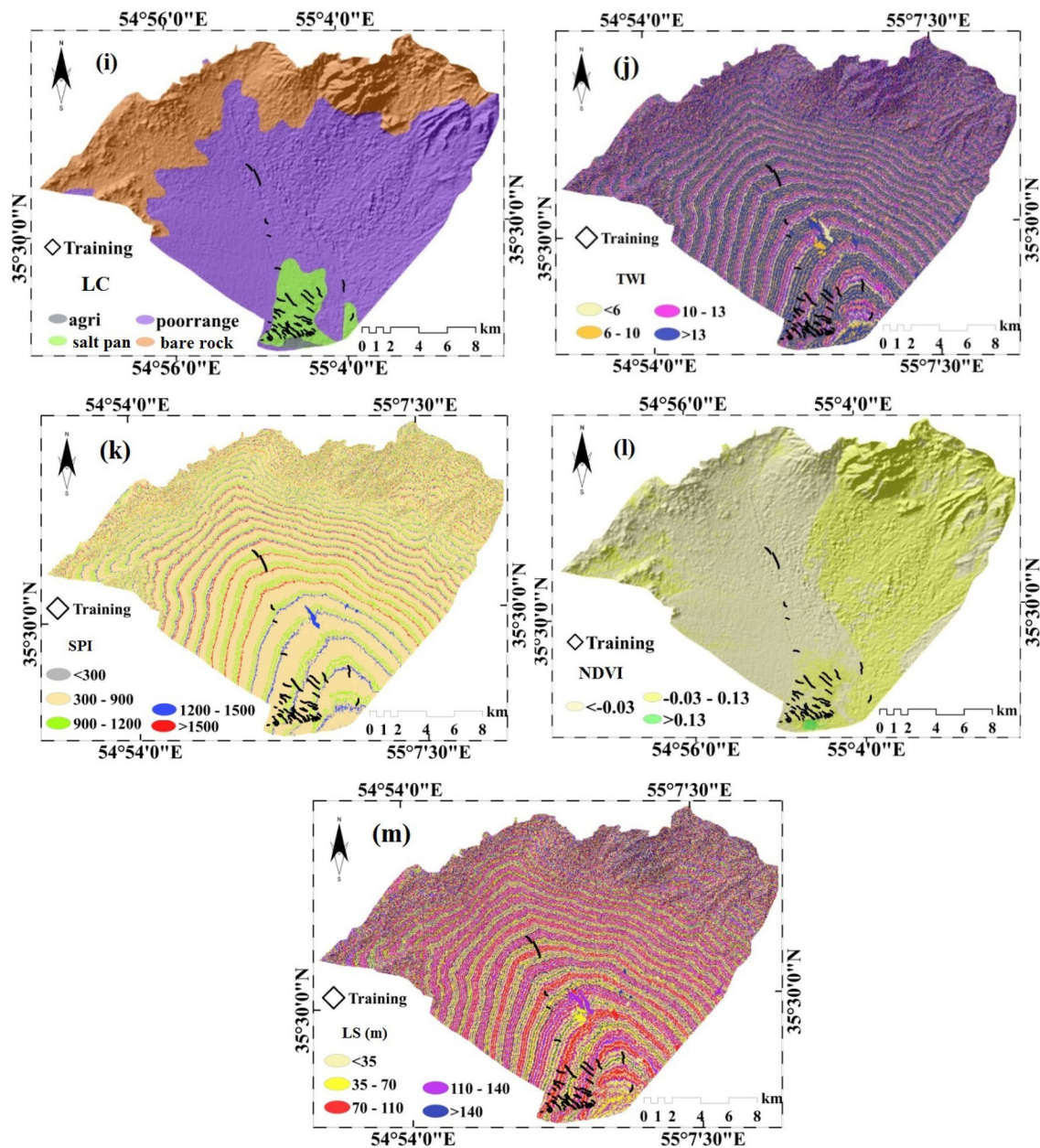


Fig. 4 (continued)

formations, soil characteristics, vegetation conditions, penetration rates, and degrees of gravity (Manap et al. 2014). High drainage density increases surface runoff rate and thus increases gully erosion. Drainage density map generated by Line Density Tool in ArcGIS 10.5 and its values classified into four categories (Conoscenti et al. 2014): 0.6–1.7, 1.7–2.1, 2.1–2.4, and > 2.4 km/km².

According to literature review, the distance from road is important for the occurrence of gully erosion (Conoscenti et al. 2014; Pourghasemi et al. 2017). Roads will enhance the gully erosion process using interrupt and concentrate

overland flow and draining it on downstream slopes (Conoscenti et al. 2014). The distance from road map was divided into five different buffer zones (Fig. 2h) using quantile classification (Conoscenti et al. 2014) in ArcGIS 10.5: 0–300 m, 300–600 m, 600–900 m, 900–1200 m, and > 1200 m.

The lithology layer was generated by digitizing the geological map prepared by GSDI (1997) (Geological Survey Department of Iran, Toroud Sheet at 1:100,000-scale). The lithology map according to susceptibility to soil erosion was then classified into 12 classes (Table 1).

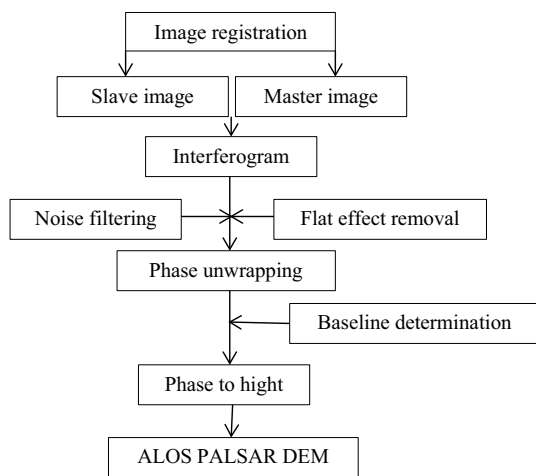


Fig. 5 InSAR data-processing procedure for DEM production

Land cover (LC) management has a great influence on the geomorphological stability of the slope and the occurrence of gully erosion (Zakerinejad and Maerker 2015). In general, bare areas and areas with scattered vegetation are more susceptible to erosion compared to forest areas, because vegetation cover significantly reduces erosive power of surface flow (Hayas et al. 2017). The LC map of the study area was generated using Landsat 8 images from 31/10/2017 covering path and row 162 and 36, respectively. To create the LC map, a supervised classification using the maximum likelihood algorithm was applied. Four LC types were extracted such as irrigation agriculture, desert, range lands, and bare rock outcrops. The produced LC was validated using 265 ground control point (GCP) in the field. Kappa coefficient for the final map was estimated by Eq. 1 (Lo and Yeung 2002):

$$K = \frac{\{N \sum_{i=1}^r (X_{ii}) - N \sum_{i=1}^r (X_{i+} \cdot X_{+i})\}}{N^2 - \sum_{i=1}^r (X_{i+} \cdot X_{+i})} \quad (1)$$

where r is number of rows in error matrix; X_{ii} is number of observations in row i and column i ; X_{i+} is total of observations in row i ; X_{+i} is total of observations in column i ; and N is total number of observations included in the matrix. Kappa coefficient of the generated map was obtained 97.65%.

The TWI has been used widely to describe the effect of topography on the location and size of saturated areas of flow surface generation (Moore et al. 1991). TWI estimate the probability of water accumulation in soil due to slope and upstream catchment area, therefore, is an important factor for assessing prone areas to gully erosion (Gómez-Gutiérrez et al. 2015). The runoff erosion power, discharge potential, and carrying capacity are modeled using the mentioned factor (Tahmassebi-poor et al. 2016). TWI computed using Eq. 2 and classified into four categories (Conforti et al. 2011): < 6, 6–10, 10–13, and > 13.

The SPI is a measure of the erosive power of water flow based on the assumption that discharge is commensurate to particular catchment area (Conforti et al. 2011). Stream power index is one of the most important factors controlling slope erosion processes. Regions with high stream power have high erosion potential (Gómez-Gutiérrez et al. 2015). SPI calculated using Eq. 3 and classified into five categories using natural break scheme (Conforti et al. 2011): < 300, 300–900, 900–1200, 1200–1500, and > 1500:

$$TWI = \ln (A_S / \tan \beta) \quad (2)$$

$$SPI = A_S \times \tan \beta, \quad (3)$$

where A_S is the specific catchment’s area (m^2/m), and β is slope gradient (in degrees).

The NDVI is a measure of surface reflectance and gives a quantitative estimation of the vegetation growth and was calculated based on Landsat 8 images, which reflects the relation between the vegetation condition and gullies (Xie

Table 1 Lithology of the study area (GSI 1997)

Code	Lithology	Formation	AGE	Area (km ²)	%
Jph	Phyllite, slate and meta-sandstone	Hamadan Phyllites	Jurassic	0.33	0.21
PIQc	Fluvial conglomerate, Piedmont conglomerate and sandstone	–	Pliocene–Quaternary	0.15	0.10
Ek	Well bedded green tuff and tuffaceous shale	Karaj	Eocene	3.79	2.44
Qft1	High level piedmont fan and valley terrace deposits	–	Quaternary	0.05	0.03
K	Cretaceous rocks in general	–	Cretaceous	14.41	9.28
Ed.avs	Dacitic-to-andesitic volcano sediment	–	Eocene	74.81	48.18
E1c	Pale-red, polygenic conglomerate and sandstone	–	Paleocene–Eocene	6.82	4.39
Qft2	Low-level piedmont fan and valley terrace deposits	–	Quaternary	0.78	0.50
Ed.avb	Dacitic-to-andesitic volcano breccia	–	Eocene	10.89	7.01
Edav	Dacitic-to-andesitic volcanic	–	Eocene	33.52	21.59
Murm	Light-red-to-brown marl and gypsiferous marl with sandstone intercalations	–	Miocene	2.79	1.79
Mur	Red marl, gypsiferous marl, sandstone, and conglomerate	Upper red	Miocene	6.95	4.48

et al. 2017). The NDVI value is calculated by the following equation:

$$NDVI = IR - R / IR + R, \tag{4}$$

where IR is the infrared portion of the electromagnetic spectrum and R is the red portion of the electromagnetic spectrum. In general, in areas with intensive vegetation, the likelihood of gully erosion is low to very low. The NDVI map of the study area classified to three classes: < - 0.039, - 0.039 to 0.13, and > 0.13 (Rahmati et al. 2016).

The length–slope parameter (LS) is a factor used in the RUSLE equation to consider the effect of topography on erosion (Renard et al. 1997). The topographical factor depends on the slope–length (L) and the slope steepness (S). This parameter is considered as a sediment transport capacity index and computed by Eq. 5 (Moore and Burch 1986):

$$LS = (f_a \times \text{cellsize}/22.13)^{0.4} \times (\sin \sigma/0.0896)^{1.3}, \tag{5}$$

where f_a is flow accumulation and σ is slope in degrees. The LS map was prepared by Raster Calculator Tool in the ArcGIS10.5 and classified to five categories (Conforti et al. 2011): < 36 m, 36–70 m, 70–110 m, 110–140 m, and > 140 m.

Analytic hierarchy process (AHP) knowledge-based technique

Because decision making according to multiple criteria is a challenging issue, the application of Multi-criteria Decision-Making Models (MCDM) was offered in different cases (Yacov and Haimes 2011). Decision-making processes are often complicated according to multiple inconsistent criteria; nevertheless, the MCDM methods have been successfully engaged to identify favorite policy alternatives (Kim and Chung 2013). The application of MCDM methods in various fields of natural hazards has been illustrated in a number of international literatures (Chitsaz and Banihabib 2015; Chen et al. 2016; Wen et al. 2017). AHP is a multi-criteria, multi-objective, and semi-quantitative method that were introduced by Saaty (1980). In this method, decision-making

weights are assigned based on expert knowledge and their experience in a form of pairwise relative comparison (Bathrellos et al. 2017; Papadakis and Karimalis 2017). Over the past two decades, the practical nature of AHP has led to the use of it on the large and complex decision-making problems (Bathrellos et al. 2012, 2016). In general, AHP consists of the following steps:

Step 1: structuring of the decision problem into a hierarchical model. A simple AHP model has three levels such as goal, criteria, and alternatives.

Step 2: making pairwise comparisons and obtaining the judgmental matrix. Bogdanovic et al. (2012) stated that a pair comparison has to start with a question on behalf decision makers. For example, depending on the purpose of the decision, the importance of the criteria to each other must assign with scales 1–9. Vidal et al. (2010) also stated that the mean numbers 2, 4, 6, and 8 have to use to correct the comparison (Table 2).

Step 3: calculation of the weight of each criterion and alternative (local priority). Local weights of criteria and alternatives were obtained according to Eqs. 6 and 7 (Macharis et al. 2004):

$$a_{ij} = a_j / \sum_{i=1}^n a_j \quad a_j, j = 1, 2, 3 \dots, n \tag{6}$$

$$w_{ij} = \sum_{i=1}^n a_{ij} / n, \quad a_{ij} = 1, 2, \dots, n, \tag{7}$$

where a_j is the values of each inline of column, a_{ij} is the normalized values of each of the in lines, and n is number of criteria.

Step 4: computation of the overall priority (final weight) by the following equation:

$$AHP_{Score} = \sum_{j=1}^n w_{ij} \times W_j, \tag{8}$$

Table 2 Scale of preference between two factors in AHP (Saaty 1980)

Preference factor	Degree of preference	Definition
1	Equally	Two activities contribute equally to the Objective
3	Moderately	Experience and judgment slightly to moderately favor one activity over another
5	Strongly	Experience and judgment strongly or essentially favor one activity over another
7	Very strongly	An activity is strongly favored over another and its dominance is showed in practice
9	Extremely	The evidence of favoring one activity over another is of the highest degree possible of an affirmation
2,4,6,8	Intermediate	Used to represent compromises between the references in weights 1, 3, 5, 7, and 9

where w_{ij} is local priority for i th alternatives in j th criteria and W_j is local priority for j th criteria.

Step 5: computation of the inconsistency index by the following equation:

$$I.I = \frac{\lambda_{\max} - n}{n - 1}, \tag{9}$$

where λ_{\max} is maximal eigen value and n is number of alternatives.

Step 6: calculation of the inconsistency ratio by the following equation:

$$IR = \frac{II}{RII}, \tag{10}$$

where RII is called random index and is obtained from Table 3. A value of IR less than 0.1 is considered acceptable (Saaty 1980), because human judgments are not always indistinct and there may be because of the nature of scale used, would have existed inconsistencies. The ability to identify inconsistent judgments through the calculation of consistency ratio is considered as one of the strong points of AHP (Table 3).

Data-driven models

Frequency ratio (FR)

Frequency ratio is a bivariate statistical method and a simple geospatial assessment tool (Wang and Li 2017) for computing the probabilistic relationship between dependent (gully inventory map) and independent variables (geo-environmental factors) and is very useful and efficient (Rahmati et al. 2016). The FR can be described as Eq. 11 (Oh et al. 2017):

$$FR = ((A/B)/(C/D)), \tag{11}$$

where A is the number of pixels with gully erosion for each class of geo-environmental factors, B is the number of total gullies in study area, C is the number of pixels in each class of the geo-environmental factors, and D is the number of total pixels in the study area.

Index of entropy (IOE)

Theory of entropy expresses the extent of the disorder, instability, uncertainty, and imbalance of a system (Al-Abadi 2017). This theory was introduced by Boltzmann and quantitatively presented by Shannon (1948) (Pourghasemi et al. 2012). Actually, theory of entropy expresses a way to

approximate main parameters among efficient parameters of a goal; in the other words, this theory characterizes variables that are more effective in phenomenon occurrence. Details of the mentioned theory and its equations are given in Pourghasemi et al. (2012), Jaafari et al. (2014), Al-Abadi (2017), and Hong et al. (2017).

After computation of the final weight of each factor and multiplying it in categories of that parameter and values related to each parameter, weighted maps were added up and the final map of gully erosion susceptibility was obtained using Eq. 12 (Haghizadeh et al. 2017):

$$GESM = \sum_{l=1}^n (W_j \times P_j), \tag{12}$$

where W_j and P_j are the final weight and the probability density for the j th feature.

Weights-of-evidence (WofE)

The WofE is one of the bivariate and statistical approaches that employed the log-linear form of the Bayesian probability method to estimate the relative importance of effective factors by statistical means (Xie et al. 2017). The WofE model calculates the relationship of between gully erosion-conditioning factors and gully occurrence according to the presence or the absence of the gullies in the study area (Razavizadeh et al. 2017) as follows:

$$W_i^+ = \log_e [(N_{pix1}/(N_{pix1} + N_{pix2})) / (N_{pix3}/(N_{pix3} + N_{pix4}))] \tag{13}$$

$$W_i^- = \log_e [(N_{pix2}/(N_{pix1} + N_{pix2})) / (N_{pix4}/(N_{pix3} + N_{pix4}))], \tag{14}$$

where N_{pix1} is number of gully erosion pixels in a specific class, N_{pix2} is (total number of gully erosion pixels in a map) – (number of gully erosion pixels in a class), N_{pix3} is (number of pixels in specific class) – (number of gully erosion pixels in a specific class), and N_{pix4} is (total number of pixels in a map) – (total number of gully erosion pixels in map) – (number of pixels in specific class). A positive weight W_i^+ indicates that the gully erosion-conditioning factor exists at the locations of gully erosion and there is a positive correlation between the presence of the gully erosion-conditioning factor and the gully locations and vice versa. Final weight in the weights-of-evidence model obtained by Eq. 15 (Rahmati et al. 2016; Razavizadeh et al. 2017):

$$W = \left(\frac{C}{S(C)} \right) \tag{15}$$

Table 3 Random index (Saaty and Vargas 2001)

No. criteria	1	2	3	4	5	6	7	8	9	10	11	12
R.I.I	0.00	0.00	0.58	0.90	1.12	1.24	1.32	1.41	1.45	1.49	1.51	1.56

$$C = W^+ + W^- \tag{16}$$

$$S(C) = \sqrt{S^2(W^+) + S^2(W^-)} \tag{17}$$

$$S^2(W^+) = \frac{1}{N\{B \cap L\}} + \frac{1}{\{B \cap L\}} \tag{18}$$

$$S^2(W^-) = \frac{1}{\{\bar{B} \cap L\}} + \frac{1}{\{\bar{B} \cap \bar{L}\}}, \tag{19}$$

where W is final weight, and C is difference between positive and negative weights. C is negative for a negative correlation between GEFs and GESM and positive for a positive relationship (Pourghasemi et al. 2013). $S(C)$ is the standard deviation of the contrast. $S^2(W^+)$ is the variance of W^+ and $S^2(W^-)$ is the variance of W^- . B and \bar{B} indicate the presence and absence of the GEFs, respectively. L is the presence of gully, and \bar{L} is the absence of a gully. After calculation the weight of each factor by WofE model, gully erosion susceptibility map (GESM) obtained by the following equation:

$$GESM = \sum_{R=1}^{R=N} W. \tag{20}$$

Results

Multi-collinearity analysis

In general, for GESM, considering of multi-collinearity of conditioning factors (GEFs) is essential. Multi-collinearity indicates a linear correlation that exists among factors. In this research, for checking multi-collinearity, the tolerance (TOL) and variance inflation factor (VIF) indices are used when values of TOL and VIF are ≤ 0.1 and ≥ 5 or 10 indicate multi-collinearity among independent variables, respectively (Park et al. 2017). The results of the multi-collinearity analysis among 18 gully erosion-conditioning factors used in this study are presented in Table 4. This analysis showed that the TOL and VIF of 13 variables including elevation, slope degree, slope aspect, plan curvature, distance from river, drainage density, distance from road, lithology, LC, TWI, SPI, NDVI, and slope-length (LS) were ≥ 0.1 and ≤ 10 , respectively. As a result, these parameters are used for preparing the final GESMs by four models.

Applying AHP model

The relative weight of gully erosion-conditioning factors obtained from pairwise comparison matrix is shown in Table 5. Based on Table 5, it can be seen that the lithology, slope, and NDVI with a values of 0.222, 0.176, and 0.137

Table 4 Multi-collinearity Analysis among gully erosion-conditioning factors

Factors	Collinearity statistics	
	Tolerance	VIF
LS	0.464	2.154
Lithology	0.644	1.552
NDVI	0.489	2.044
Plan curvature	0.518	1.929
LC	0.633	1.581
SPI	0.283	3.529
TWI	0.209	4.786
Rain	0.049	20.208
Slope	0.274	3.648
Dense stream	0.337	2.967
Dis-stream	0.145	6.919
elevation	0.651	1.535
Convergence index	0.099	10.115
Aspect	0.614	1.629
Soil texture	0.035	28.78
Dis-fault	0.023	34.7
Dis-road	0.456	5.32
Profile curvature	0.05	15.56

are the most important factors, respectively. This result is in line with Golestani et al. (2014), Gomez-Gutierrez et al. (2009), and Rahmati et al. (2016). Gómez-Gutiérrez et al. (2015) stated that vegetation cover strongly reduces the erosive of flow surface and as a result have a high effect in gully erosion occurrence. Golestani et al. (2014) proved that the areas with gentle slope are susceptible for surface flow accumulation and gully erosion. Rahmati et al. (2016) indicated that the lithology properties are very important in gully erosion. In contrast, factors of aspect, plan curvature, and TWI with score values of 0.019, 0.015, and 0.012 had the lowest impact on the gully erosion, respectively. Factors of LC, elevation, distance from road, drainage density, SPI, LS, and distance from stream are located in the ranks of 4 to 10. The inconsistency ratio (IR) for pairwise comparison matrix of criteria is obtained 0.032; the ratio indicates an appropriate degree of inconsistency for this approach (modeling by AHP). In addition, the relationship among the gully erosion locations and the classes of conditioning factors are presented in Table 6. By the way, the inconsistency ratio (IR) for each pairwise comparison matrix is shown in Table 6. According to Table 5, all IR values are less than 0.1. After computation of weights of criteria and their classes, to GESM using AHP, Eq. 21 is used in ArcGIS10.5 by Weighted Tool as follows:

Table 5 Relationship between gully erosion and gully conditioning factors using IOE and AHP models

Factors	Classes	Domain pixels (%)	Gully pixels (%)	IOE					AHP		
				(P_{ij})	H_j	I_j	Mean P_{ij}	W_j	W classes		$W_{factors}$
									W	IR	
Elevation (m)	< 850	31.07	91.59	0.91	0.00	0.87	0.65	0.96	0.50	0.032	0.085
	850–950	29.47	8.41	0.09	0.31				0.26		
	950–1050	25.20	0.00	0.00	0.00				0.13		
	1050–1150	11.69	0.00	0.00	0.00				0.07		
	> 1150	2.57	0.00	0.00	0.00				0.03		
Slope (°)	< 5	63.83	93.97	0.83	0.23	1.26	0.30	0.37	0.95	0.053	0.176
	5–10	19.57	6.03	0.17	0.44				0.03		
	10–15	8.69	0	0.00	0.00				0.01		
	15–20	4.22	0	0.00	0.00				0.00		
	20–30	2.32	0	0.00	0.00				0.00		
	> 30	1.37	0	0.00	0.00				0.00		
Aspect	F	4.46	13.71	0.34	0.53	0.38	1.00	0.38	0.34	0.064	0.019
	N	7.84	7.31	0.10	0.00				0.10		
	NE	15.41	18.10	0.13	0.38				0.13		
	E	17.21	24.31	0.16	0.42				0.16		
	SE	18.62	22.85	0.14	0.39				0.14		
	S	16.64	9.69	0.06	0.00				0.06		
	SW	9.75	1.83	0.02	0.12				0.02		
	W	6.31	1.46	0.03	0.00				0.03		
Plan curvature (100/m)	Concave	37.75	37.66	0.33	0.53	0.34	1.01	0.34	0.32	0.025	0.015
	Flat	29.49	40.22	0.45	0.52				0.50		
	Convex	32.76	22.12	0.22	0.00				0.18		
Dis-stream	0–100	40.14	47.90	0.29	0.52	0.05	0.83	0.04	0.29	0.075	0.024
	100–200	28.92	27.24	0.23	0.49				0.23		
	200–300	19.24	18.46	0.23	0.49				0.23		
	300–400	6.46	4.94	0.18	0.45				0.18		
	> 400	5.25	1.46	0.07	0.26				0.07		
Drainage density (m/m ²)	0.6–1.7	24.92	0.00	0.00	0.00	0.81	0.48	0.39	0.05	0.062	0.052
	1.7–2.1	24.91	6.03	0.13	0.38				0.10		
	2.1–2.4	25.45	42.60	0.87	0				0.26		
	> 2.4	24.72	51.37	1.08	0				0.59		
Dis-road (m)	0–300	5.01	37.29	0.51	0.50	0.20	2.92	0.60	0.51	0.043	0.067
	300–600	4.95	12.25	0.17	0.43				0.17		
	600–900	4.43	13.35	0.21	0.47				0.21		
	900–1200	3.81	4.94	0.09	0.31				0.09		
	> 1200	81.80	32.18	0.03	0.14				0.03		

Table 5 (continued)

Factors	Classes	Domain pixels (%)	Gully pixels (%)	IOE					AHP		
				(P_{ij})	H_j	I_j	Mean P_{ij}	W_j	W classes		$W_{factors}$
									W	IR	
Lithology	Jph	4.61	0	0	0	0.82	2.19	1.79	0.00	0.052	0.226
	PIQc	7.96	22.26	0.11	0				0.10		
	Ek	0.91	0	0	0				0.00		
	Qft1	1.58	27.37	0.66	0.40				0.63		
	K	4.42	0	0	0				0.01		
	Ed.avs	17.97	0	0	0				0.01		
	E1c	2.76	0	0	0				0.01		
	Qft2	46.77	45.26	0.04	0				0.04		
	Ed.avb	2.62	0	0	0				0.01		
	Edav	8.05	0	0	0				0.01		
	Murm	0.67	2.37	0.13	0				0.12		
	Mur	1.67	2.74	0.06	0.25				0.06		
LC	Agriculture	0.34	0	0	0	0.98	3.93	3.86	0.12	0.068	0.108
	Salt pan	4.99	76.46	0.98	0.04				0.58		
	Range	60.76	23.54	0.02	0.00				0.26		
	Bare rock	33.91	0.00	0.00	0.00				0.05		
TWI	< 6	7.63	7.86	0.33	0.00	0.74	0.79	0.58	0.30	0.035	0.012
	6–10	26.81	26.33	0.31	0.52				0.18		
	10–13	15.36	17.55	0.36	0.00				0.50		
	> 13	50.20	48.26	0.30	0.00				0.02		
SPI	< 300	0.01	0	0.00	0.00	0.19	0.56	0.107	0.27	0.039	0.04
	300–900	81.97	87.39	0.38	0.53				0.31		
	900–1200	11.23	9.32	0.29	0.52				0.08		
	1200–1500	3.91	2.38	0.22	0.48				0.13		
	> 1500	2.88	0.91	0.11	0.35				0.21		
NDVI	< - 0.039	53.63	21.57	0.005	0.040	0.44	0.69	0.304	0.98	0.063	0.137
	- 0.039 to 0.13	46.21	66.54	0.019	0.109				0.02		
	> 0.13	0.16	11.88	0.98	0				0.01		
LS (m)	< 36	28.64	29.43	0.21	0.00	0.81	0.97	0.78	0.04	0.06	0.031
	36–70	18.04	16.27	0.19	0.45				0.09		
	70–110	17.57	24.68	0.29	0.00				0.15		
	110–140	21.52	23.95	0.23	0.00				0.25		
	> 140	14.24	5.67	0.08	0.00				0.47		

$$\begin{aligned}
 GESM_{AHP} = & [(elevation_w \times 0.085) + (slope_w \times 0.176) \\
 & + (aspet_w \times 0.019) + (plan\ curvature_w \times 0.015) \\
 & + (dis\ stream_w \times 0.024) + (drinage\ density_w \times 0.052) \\
 & + (dis\ road_w \times 0.067) + (lithology_w \times 0.226) \\
 & + (LC_w \times 0.085) + (TWI_w \times 0.012) + (SPI_w \times 0.04) \\
 & + (NDVI_w \times 0.137) + (LS_w \times 0.031)] \quad (21)
 \end{aligned}$$

The results of gully erosion susceptibility map produced by AHP method are shown in Fig. 6a. It has reclassified into five susceptibility classes: very low, low, moderate, high, and very high based on natural break classification

method (Xie et al. 2017). According to Fig. 6a, the very high susceptibility level is located in the south part of the study area. This area covered with Qft1 and Qft2 that have sensitive lithological units to erosion. In contrast, very low gully erosion susceptible areas widely distributed in the northern parts of area due to the Outburst of igneous rocks and low depth of soil. Area of the susceptibility classes are shown in Table 6. Based on Table 6, from total of the study area (416.82 km²), 17.5% (72.88 km²) is located in very low susceptibility class, 22.86% (95.20 km²) in low susceptibility, 25.49% (106.16 km²) in moderate susceptibility, 28.31% (117.9 km²) in high, and 5.85% (24.36 km²) in very high susceptibility class.

Table 6 Area percentage of the susceptibility classes in different models. Gully cells training set and gully cells testing set falling in each susceptibility class and SCAI values

	Susceptibility classes	Area (km)		Gully training set		Gully validation set		All gully set (%)	SCAI
		Area	%	Area	%	Area	%		
AHP	Very low	72.88	17.50	0	0	0	0	0	0
	Low	95.20	22.86	0	0	0	0	0	0
	Moderate	106.16	25.49	0	0.55	0	0	0.55	45.97
	High	117.90	28.31	0.12	23.84	0.07	23.77	47.61	0.59
	Very high	24.36	5.85	0.37	75.60	0.24	76.23	151.83	0.04
FR	Very low	107.61	25.82	0	0	0	0	0	0
	Low	44.25	10.62	0	0	0	0	0	0
	Moderate	149.82	35.94	0	0.18	0	0	0.47	76.45
	High	109.97	26.38	0.38	77.33	0.25	81	158.65	0.17
	Very high	5.16	1.24	0.11	22.49	0.06	18	40.88	0.03
IOE	Very low	69.75	16.75	0	0	0	0	0	0
	Low	76.97	18.48	0	0	0	0	0	0
	Moderate	135.40	32.51	0	0.92	0.05	15.07	16.00	2.03
	High	123.93	29.76	0.23	46.77	0.15	48.99	95.75	0.31
	Very high	10.45	2.51	0.25	52.31	0.11	35.94	88.25	0.03
WofE	Very low	21.24	5.10	0	0	0	0	0	0
	Low	126.61	30.40	0	0	0	0	0	0
	Moderate	181.89	43.67	0.01	2.40	0.03	10.14	12.55	3.48
	High	71.35	17.13	0.20	40.48	0.15	47.25	87.73	0.20
	Very high	15.40	3.70	0.28	57.12	0.13	42.61	99.73	0.04

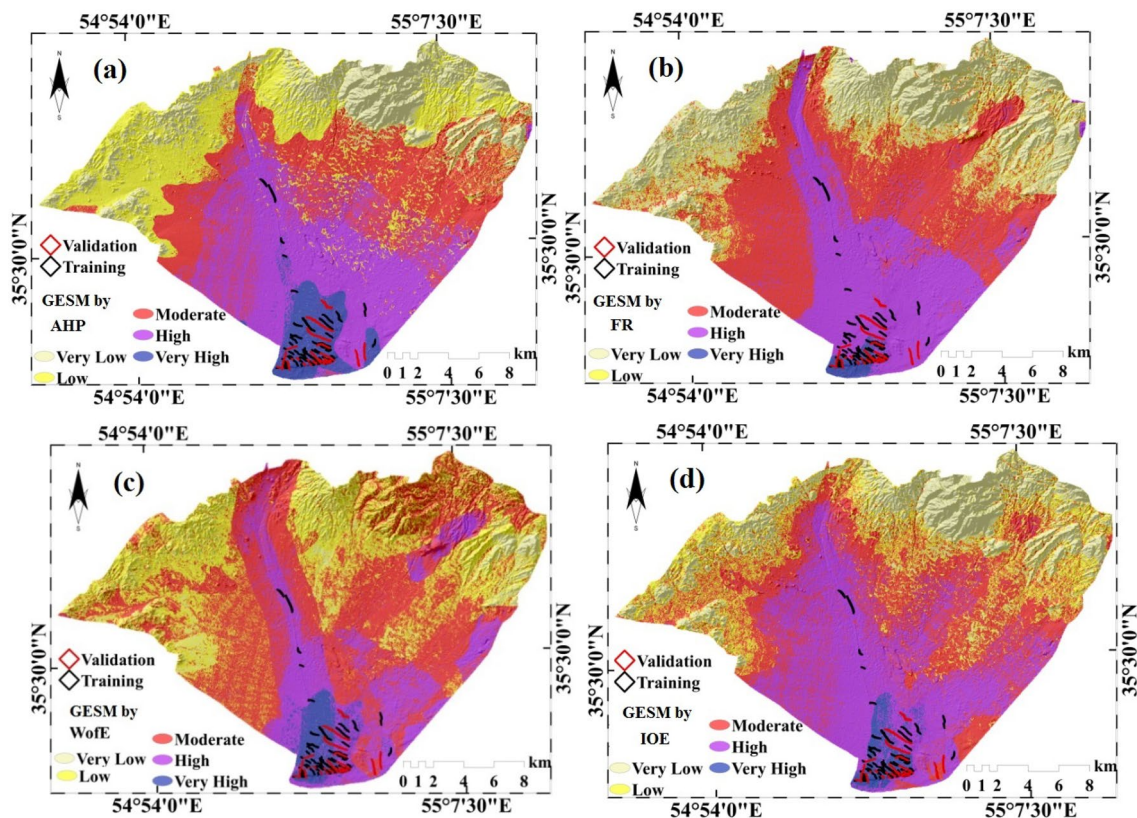


Fig. 6 Gully erosion susceptibility maps **a** AHP, **b** FR, **c** WofE, and **d** IOE

Applying FR model

The FR values were estimated based on spatial relationship of gully erosion locations and 13 conditioning factors. As shown in Table 7, when a class of a factor has the FR value higher than 1, it may be assumed that the class is susceptible to gully erosion. Application of the frequency ratio model showed that most gully erosion locations are located at elevations of <916 m. Elevation class <916 m has the highest FR value of 2.95, followed by 916–1065 m. Elevations higher than 1065 m had the lowest frequency ratio (0.00). Rahmati et al. (2016) stated that gully distribution is mainly controlled by topographic factors such as elevation. In the case of slope degree, it could be seen that the classes of <5° had higher FR values (1.47), followed by 5°–10°. In Slope degree higher than 10°, gully erosion has not observed. This result is in line with Ghorbani Nejad et al. (2016) that proved light slopes because of surface flow accumulation, increases the likelihood of gully erosion occurrence. The FR trend of the slope aspect factor showed that classes of flat, east, northeast, and southeast with FR higher than 1 have a clear positive correlation with gully erosion and flat faces with higher FR value (3.08) have the most correlation with gully occurrence. This result is in line with Rahmati et al. (2016). For plan curvature factor, flat areas proved to be the most susceptible to gully erosion with the highest FR value of 1.36. The concave and convex classes had the lowest FR values (1 and 0.68), respectively. The relationship between distance from river and gullies revealed that there is a strong and indirect correlation between them. Class of 0–100 m had the highest FR value (1.19), followed by 200–300 m, 100–200 m, 300–400 m, and >400 m. The spatial relationship between gullies with drainage density revealed that high FR value is related to high and very high density areas and gully erosion was not occur at drainage density lower than 1.7 km/km². In addition, results showed that class >2.4 km/km² with the highest density, had the highest FR value (2.08) and had the strongest relationship with gully erosion susceptibility. The correlation between the gully locations and the distance from road showed that the class less than 300 m had the highest FR weight (7.45), expresses high gully erosion susceptibility in this range of distance from road. In contrast, classes >1200 m with the lowest FR value (0.39) had a weak relation with gully erosion. For the geology factor, the high level piedmont fan and valley terrace deposits class had the highest FR value (7.32), indicating high susceptibility in this area, followed by light-red-to-brown marl and Gypsiferous marl with sandstone intercalations and fluvial conglomerate, piedmont conglomerate, and sandstone with FR values of 3.27 and 2.80, respectively. For the LC, it can be seen that the salt pan class has FR value of 13.35, showed that the gully erosion susceptibility in this LC is high. The analysis of FR model for the relationship between gully

erosion locations and TWI showed that class of 10–13 with the highest FR (1.14) had strong influences on gully erosion occurrence. For the SPI factor, the class 300–900 had the highest FR value (1.07), followed by classes 900–1200 with FR (0.83). In the case of NDVI, class of –0.039 to 0.13 with highest FR (1.44) had strong relation with gully erosion. For the LS factor, class of 70–110 m, 110–144 m, and <36 m with FR values of higher than 1, represent strong relation with gully erosion. Finally, In order to generate a gully erosion susceptibility map, the GESM was calculated by summing each weighted factor using the following equation:

$$\begin{aligned} \text{GESM}_{\text{FR}} = & [(\text{elevation}_{\text{FR}}) + (\text{slope}_{\text{FR}}) + (\text{aspect}_{\text{FR}}) \\ & + (\text{plan curvature}_{\text{FR}}) + (\text{dis stream}_{\text{FR}}) \\ & + (\text{drainage density}_{\text{FR}}) + (\text{dis road}_{\text{FR}}) \\ & + (\text{lithology}_{\text{FR}}) + (\text{LU/LC}_{\text{FR}}) + (\text{TWI}_{\text{FR}}) \\ & + (\text{SPI}_{\text{FR}}) + (\text{NDVI}_{\text{FR}}) + (\text{LS}_{\text{FR}})]. \quad (22) \end{aligned}$$

FR model provides values of GEMS ranging from 3.32 to 115.12. The gully erosion map was divided into five susceptibility classes include very low, low, moderate, high, and very high (Fig. 6b) using the natural breaks method (Cao et al. 2016). Each class in the study was consisted of 25.82%, 10.62%, 35.94%, 26.38%, and 1.24% of total study area, respectively (Table 6). The mean and standard deviation of this model are 6.12 and 7.21. Most of the high and very high susceptibility classes are located in the south part of study area because of the high lineament density, lower slope, and prone nature of surface and subsurface materials for gully erosion.

Applying weight of evidence model

To apply the WoE modeling, map of every factor is crossed with the GIM using the ArcGIS 10.5, and the density of the gullies calculated in each class. The resultant weights and the spatial relationship between the gully erosion occurrence and classes of each conditioning factor based on WofE model are shown in Table 7. Negative weights indicate negative spatial relationship and positive weights indicate a positive relationship between gully erosion locations and conditioning factor. Classes with positive weights are prone area for gully erosion and vice versa. To generate the final GESM map, weight of classes of each conditioning factor is summed using Eq. 23 in the weighted sum option by Spatial Analyst Tool in ArcGIS 10.5 (Fig. 6c). The final produced GESM by WofE model ranges from about –98.32 to 199.17. Obviously, larger GESM values indicate a higher susceptibility to gully erosion. The produced map based on these values was classified into five classes including very low, low, moderate, high, and very high using the natural break method (Xie et al. 2017). The areas in the very low,

Table 7 Relationship between gully erosion and 13 conditioning factors using FR and WofE models

Factors	Classes	Pixels in domain		Gully pixels		FR	Weight of evidence (WofE)				
		No	%	No	%		w+	w-	C	S [⊙]	W
Elevation (m)	<916	144,184	31.07	501	91.59	2.95	1.08	- 2.10	3.19	0.15	20.69
	916–1065	136,753	29.47	46	8.41	0.29	- 1.25	0.26	- 1.52	0.15	- 9.84
	1065–1229	116,939	25.20	0	0	0	0	0.29	- 0.29	0.04	- 6.80
	1229–1473	54,252	11.69	0	0	0	0	0.12	- 0.12	0.04	- 2.91
	> 1473	11,917	2.57	0	0	0	0	0.03	- 0.03	0.04	- 0.61
Slope (°)	<5	296,189	63.83	514	93.97	1.47	0.39	- 1.79	2.18	0.18	12.14
	5–10	90,815	19.57	33	6.03	0.31	- 1.18	0.16	- 1.33	0.18	- 7.42
	10–15	40,342	8.69	0	0	0	0	0.09	- 0.09	0.04	- 2.13
	15–20	19,587	4.22	0	0	0	0	0.04	- 0.04	0.04	- 1.01
	20–30	10,752	2.32	0	0	0	0	0.02	- 0.02	0.04	- 0.55
> 30	6360	1.37	0	0	0	0	0.01	- 0.01	0.04	- 0.32	
Aspect	F	20,691	4.46	75	13.71	3.08	1.13	- 0.10	1.23	0.12	9.88
	N	36,378	7.84	40	7.31	0.93	0	0.01	- 0.01	0.04	- 0.13
	NE	71,504	15.41	99	18.10	1.17	0	- 0.03	0.03	0.05	0.68
	E	79,841	17.21	133	24.31	1.41	0.35	- 0.09	0.44	0.10	4.38
	SE	86,401	18.62	125	22.85	1.23	0.21	- 0.05	0.26	0.10	2.54
	S	77,240	16.64	53	9.69	0.58	0	0.08	- 0.08	0.04	- 1.78
	SW	45,242	9.75	10	1.83	0.19	0	0.08	- 0.08	0.04	- 1.95
	W	29,298	6.31	8	1.46	0.23	0	0.05	- 0.05	0.04	- 1.17
Plan curvature (100/m)	NW	17,450	3.76	4	0.73	0.19	0	0.03	- 0.03	0.04	- 0.72
	Concave	175,174	37.75	206	37.66	1.00	0.00	0.00	0.00	0.09	- 0.04
	Flat	136,839	29.49	220	40.22	1.36	0.31	- 0.17	0.48	0.09	5.46
Dis-stream	Convex	152,032	32.76	121	22.12	0.68	- 0.39	0.15	- 0.54	0.10	- 5.24
	0–100	186,250	40.14	262	47.90	1.19	0.18	- 0.14	0.32	0.09	3.69
	100–200	134,216	28.92	149	27.24	0.94	- 0.06	0.02	- 0.08	0.10	- 0.87
	200–300	89,259	19.24	101	18.46	0.96	0	0.01	- 0.01	0.05	- 0.20
	300–400	29,954	6.46	27	4.94	0.76	0	0.02	- 0.02	0.04	- 0.37
> 400	24,362	5.25	8	1.46	0.28	0	0.04	- 0.04	0.04	- 0.91	
Drainage density (m/m ²)	0.6–1.7	115,633	24.92	0	0.00	0.00	0	0.29	- 0.29	0.04	- 6.71
	1.7–2.1	115,588	24.91	33	6.03	0.24	- 1.42	0.22	- 1.64	0.18	- 9.15
	2.1–2.4	118,095	25.45	233	42.60	1.67	0.52	- 0.26	0.78	0.09	8.99
	> 2.4	114,725	24.72	281	51.37	2.08	0.73	- 0.44	1.17	0.09	13.68
Dis-road (m)	0– 300	23,233	5.01	204	37.29	7.45	2.02	- 0.42	2.43	0.09	27.50
	300–600	22,969	4.95	67	12.25	2.47	0.91	- 0.08	0.99	0.13	7.57
	600–900	20,573	4.43	73	13.35	3.01	0	- 0.10	0.10	0.05	2.13
	900–1200	17,696	3.81	27	4.94	1.29	0	- 0.01	0.01	0.04	0.27
	> 1200	379,570	81.80	176	32.18	0.39	0	1.32	- 1.32	0.05	- 25.40

Table 7 (continued)

Factors	Classes	Pixels in domain		Gully pixels		FR	Weight of evidence (WofE)				
		No	%	No	%		w+	w-	C	S [⊗]	W
Lithology	Jph	21,343	4.61	0	0	0	0	0.05	0	0	0
	PIQc	36,827	7.96	122	22.30	2.80	1.03	-0.17	1.20	0.10	11.70
	Ek	4209	0.91	0	0	0	0	0.01	0	0	0.00
	Qft1	7323	1.58	150	27.42	17.32	2.87	-0.30	3.18	0.10	33.14
	K	20,435	4.42	0	0	0	0	0.05	0	0	0
	Ed.avs	83,112	17.97	0	0	0	0	0.20	0	0	0
	E1c	12,773	2.76	0	0	0	0	0.03	-0.03	0.04	-0.66
	Qft2	216,334	46.77	248	45.34	0.97	-0.03	0.03	-0.06	0.09	-0.67
	Ed.avb	12,098	2.62	0	0	0	0	0.03	0	0	0
	Edav	37,232	8.05	0	0	0	0	0.08	0	0	0
	Murm	3100	0.67	12	2.19	3.27	1.19	-0.02	1.20	0.29	4.12
	Mur	7715	1.67	15	2.74	1.64	0.50	-0.01	0.51	0.26	1.94
LC	Agriculture	1553	0.34	0	0	0	0	0	0	0.04	-0.08
	Salt pan	23,077	4.99	419	76.60	15.35	2.75	-1.40	4.15	0.10	41.10
	Range	281,023	60.76	128	23.40	0.39	-0.95	0.67	-1.62	0.10	-16.09
	Bare rock	156,848	33.91	0	0	0	0	0.41	0	0	0
TWI	<6	35,395	7.63	43	7.86	1.03	0	0.00	0.00	0.04	0.06
	6-10	124,428	26.81	144	26.33	0.98	-0.02	0.01	-0.03	0.10	-0.26
	10-13	71,269	15.36	96	17.55	1.14	0.13	-0.03	0.16	0.11	1.42
	>13	232,953	50.20	264	48.26	0.96	-0.04	0.04	-0.08	0.09	-0.91
SPI	<300	67	0.01	0	0	0	0	0.00	0.00	0.04	0.00
	300-900	380,374	81.97	478	87.39	1.07	0.06	-0.36	0.42	0.13	3.27
	900-1200	52,106	11.23	51	9.32	0.83	0	0.02	-0.02	0.04	-0.47
	1200-1500	18,131	3.91	13	2.38	0.61	0	0.02	-0.02	0.04	-0.37
	>1500	13,367	2.88	5	0.91	0.32	0	0.02	-0.02	0.04	-0.47
NDVI	<-0.039	248,854	53.63	118	21.57	0.62	-0.47	0.36	-0.83	0.09	-9.20
	-0.039 to 0.13	214,442	46.21	364	66.54	1.44	0.37	-0.48	0.84	0.09	9.27
	>0.13	749	0.16	65	11.88	0	0.00	0.00	0.00	0.04	-0.04
LS (m)	<36	132,893	28.64	161	29.43	1.03	0.03	-0.01	0.04	0.09	0.41
	36-70	83,721	18.04	89	16.27	0.90	-0.10	0.02	-0.12	0.12	-1.08
	70-110	81,518	17.57	135	24.68	1.40	0	-0.09	0.09	0.05	1.83
	110-140	99,840	21.52	131	23.95	1.11	0	-0.03	0.03	0.05	0.64
	>140	66,073	14.24	31	5.67	0.40	0	0.10	-0.10	0.04	-2.17

low, moderate, high, and very high gully erosion susceptibility classes were 5.10% (21.24 km²), 30.40% (126.61 km²), 43.67% (181.89 km²), 17.13% (71.35 km²), and 3.70% (15.40 km²), respectively:

$$\begin{aligned}
 \text{GESM}_{\text{WofE}} = & [(elevation_{\text{WofE}}) + (slope_{\text{WofE}}) \\
 & + (aspet_{\text{WofE}}) + (plan\ curvature_{\text{WofE}}) \\
 & + (dis\ stream_{\text{WofE}}) + (drainage\ density_{\text{WofE}}) \\
 & + (dis\ road_{\text{WofE}}) + (lithology_{\text{WofE}}) \\
 & + (LU/LC_{\text{WofE}}) + (TWI_{\text{WofE}}) + (SPI_{\text{WofE}}) \\
 & + (NDVI_{\text{WofE}}) + (LS_{\text{WofE}})]. \quad (23)
 \end{aligned}$$

Applying index of entropy (IOE)

The results of index of entropy model for GESM are shown in Table 5. According to it, factors of LC, lithology, and elevation with weights of 3.86, 1.79, and 0.96 have had the greatest impact on the gully erosion. In contrast, factors of distance to stream, stream power index, and NDVI with 0.04, 0.107, and 0.304 scores had the lowest impact on gully erosion, respectively. The parameters of stream length (LS), distance from road, TWI, drainage density, slope aspect, slope degree, and plan curvature are located in the next ranks. The relation between classes of parameters and gully erosion locations by index of entropy model is shown in Table 5.

The final GESM using index of entropy model was generated using the following equation:

$$\begin{aligned} \text{GESM}_{\text{shanoon}} = & [(elevation_w \times 0.71) + (slope_w \times 0.23) \\ & + (aspet_w \times 0.38) + (plan\ curvature_w \times 0.31) \\ & + (dis\ stream_w \times 0.04) \\ & + (drainage\ density_w \times 0.39) \\ & + (dis\ road_w \times 0.60) + (lithology_w \times 1.79) \\ & + (LU/LC_w \times 3.86) + (TWI_w \times 0.79) \\ & + (SPI_w \times 0.25) + (NDVI_w \times 22.79) \\ & + (LS_w \times 0.07)]. \end{aligned} \quad (24)$$

The result of this summation is a continuous interval of values from 0.96 to 8.22, which represents the gully erosion

susceptibility index. A natural break classification scheme was used to divide the values into five classes (Fig. 6d) and a susceptibility map was prepared. According to the gully erosion susceptibility map generated with the IOE model, it was found that 16.75%, 18.48%, 32.51%, 29.76%, and 2.51% of the total area falls in the very low, low, moderate, high, and very high susceptible classes, respectively.

Validation and sensitivity analysis

The success rate and prediction rate curves are used to verify the accurate of the gully erosion susceptibility results (Guo-liang et al. 2017). Validation was performed by comparison of gully locations and the produced gully erosion susceptibility maps. Both success rate and prediction rate

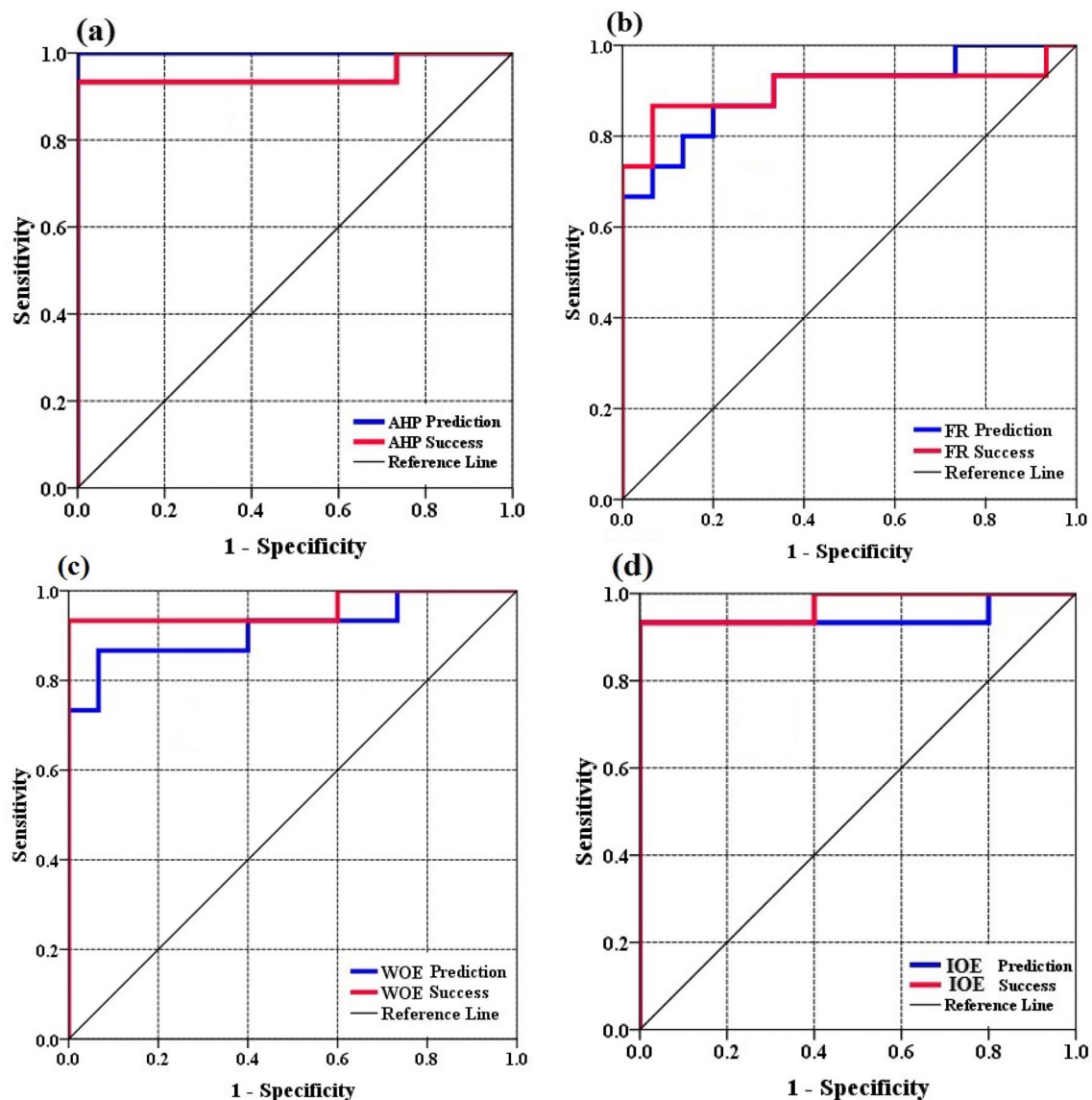


Fig. 7 Prediction and success rates a AHP, b FR, c WofE, and d IOE

Table 8 Area under the curve (AUC)

Models	Variables	Area	Standard error	Asymptotic significant	Asymptotic 95% confidence interval	
					Lower bound	Upper bound
AHP	Prediction	0.954	0.000	0.000	1.000	1.000
	Success	0.973	0.000	0.000	1.000	1.031
FR	Prediction	0.912	0.008	0.000	0.799	1.009
	Success	0.917	0.004	0.000	0.801	1.004
IOE	Prediction	0.939	0.000	0.000	0.923	1.009
	Success	0.925	0.003	0.000	0.856	1.024
WofE	Prediction	0.926	0.002	0.000	0.871	1.043
	Success	0.921	0.005	0.000	0.816	1.021

curves of the gully erosion susceptibility maps were verified using training and validating data set, respectively. These rates can assess using AUC that ranges from 0.5 to 1.0. The AUC values can be classified as follows: 0.5–0.6, poor; 0.6–0.7, average; 0.7–0.8, good; 0.8–0.9, very good; and 0.9–1, excellent (Rahmati et al. 2016). Results of success rate and prediction rate are shown in Table 8 and Fig. 7. The results showed that value of success rate is 0.973 (97.3%) for AHP model that are better than success rates of 0.917 (91.7%) FR, 0.925 (92.5%) IOE, and 0.921 (92.1%) WofE models. In addition, prediction rate of 0.954 (95.4%) using AHP model is better than prediction rates of 0.912 (92.1%) FR, 0.939 (93.9%) IOE, and 0.926 (92.6%) WofE models. Results indicated that four model had excellent performance in prediction prone areas to gully erosion and can be used as an effective method to perform gully erosion susceptibility maps. In addition, the seed cell area index (SCAI) validation technique proposed by Süzen and Doyuran (2004) was applied in this study. SCAI shows the density of gullies among the landslide susceptibility zones. In general, high and very high susceptibility classes have very small SCAI values (Pawluszek and Borkowski 2017). Results of SCAI indicator are shown in Table 6. According to Table 6, SCAI values of the four models are desirable in the high and very high susceptibility classes.

Discussion

Data-driven and knowledge-based models reflect two different perspectives in spatial modeling. A knowledge-based approach is based on field campaigns, expert knowledge and experience, evidence of varying quality, and guidelines, while a data-driven approach is based on the observational data. The advantages of AHP approach are (1) flexibility, intuitive appeal to the decision makers, and its ability to check inconsistencies, (2) the AHP method break down a decision problem into its constituent sections and builds hierarchies of criteria and calculate the importance of each

criterion, (3) AHP reduces bias in decision making by providing a useful mechanism for checking consistency of the evaluation measures and alternatives, and (4) the AHP method supports group decision making. The main disadvantages of AHP are (1) the number of pairwise comparisons may become very large in this model, and, therefore, become a difficult task, (2) the artificial limitation of the use of the 9 point scale is another disadvantage and may difficult to distinguish for decision maker that one alternative is 3 or 5 times more important than another, and (3) in AHP model, compensation between good scores on some criteria and bad scores on other criteria can occur. Therefore, important information may be missing (Macharis et al. 2004). The results of the comparison performed in this research stated that knowledge-based models such as AHP and data-driven classification methods such as FR, WofE, and IOE had the excellent (AUC = 0.9–1) prediction capabilities for identifying prone areas to soil erosion that these results are in agreement with Dube et al. (2014), Wang et al. (2015), Rahmati et al. (2016), Pawluszek and Borkowski (2016), Wu et al. (2016); and Xie et al. (2017). Dube et al. (2014) applied weights-of-evidence model for gully erosion hazard assessment in Mbire District—Zimbabwe and indicated that this model had high accuracy in prediction of prone areas to gully erosion. Wang et al. (2015) used certainty factor and index of entropy models for assessment of landslide susceptibility in the Qianyang County of Baoji City, China. Their results showed that IOE model with prediction rate of 80.88% had good accuracy in identification of susceptible areas to landslide. Rahmati et al. (2016) investigated GESM using bivariate statistical models including weights-of-evidence and frequency ratio and stated that frequency ratio model with (AUC = 78.11%) had better accuracy in comparison to WofE model (AUC = 70.07%). Pawluszek and Borkowski (2016) considered impact of DEM-derived factors and AHP model for landslide susceptibility mapping in the region of Roznow Lake, Poland. Their results indicated that AHP model had high capability in prediction of susceptible areas to landslide. Wu et al. (2016) prepared

a landslide susceptibility map using statistical index (SI), frequency ratio (FR), and certainty factor (CF) models in a Geographic Information System (GIS) for the Gangu County, Gansu Province, China and stated that FR model with prediction accuracy of 75.62% had performed better than CF model. Xie et al. (2017) compared weights-of-evidence, logistic regression, and support vector machine models and evaluated their results by SBAS-InSAR monitoring for landslide susceptibility mapping in China and showed that WofE model with prediction rate of 0.812 had good prediction capability in identifying the prone areas to landslide.

Conclusions

Gully erosion is one of the most hazards in the Toroud Watershed that it causes loss of soil and the destruction of infrastructure. Therefore, an accurate assessment of the probability of gully erosion occurrence is required for conservation of natural resources such as soil and reducing its potential risks. For this purpose, four GIS-based models such as AHP, FR, WofE, and IOE models as expert knowledge and data-driven techniques were used to generate the gully erosion susceptibility maps for the study area in Semnan Province, Iran. Performance of four models was compared by AUC and SCAI methods. To produce gully erosion susceptibility maps in the study area, among 18 geo-environmental factors selected based on literature review, data accessible, and field surveys, 13 gully erosion-conditioning factors were used for modeling purposes. The final gully susceptibility maps were classified based on natural break algorithm. Results of validation showed that the gully erosion susceptibility maps generated by four models show good prediction efficiency and the four models have been used successfully to produce gully erosion susceptibility maps for the study area. Therefore, the gully erosion susceptibility maps generated in this research are an important tool for planners, decision makers, and engineers. They can make affordable, rapid, and well-grounded decisions to minimize and avoid the damage and losses caused by existing and future gullies, or avoid the high and very high susceptible zones, by appropriate preventive measures and mitigation procedures.

Acknowledgements The study was supported by College of Agriculture, Shiraz University (Grant No. 96GRD1M271143).

References

- Achour Y, Boumezbeur A, Hadji R, Chouabbi A, Cavaleiro V, Bendaoud EA (2017) Landslide susceptibility mapping using analytic hierarchy process and information value methods along a highway road section in Constantine, Algeria. *Arab J Geosci* 10:194
- Al-Abadi AM (2017) Modeling of groundwater productivity in north-eastern Wasit Governorate, Iraq using frequency ratio and Shannon's entropy Models. *Appl Water Sci* 7: 699–716
- Bathrellos GD, Gaki-Papanastassiou K, Skilodimou HD, Papanastassiou D, Chousianitis KG (2012) Potential suitability for urban planning and industry development by using natural hazard maps and geological—geomorphological parameters. *Environ Earth Sci* 66(2):537–548
- Bathrellos GD, Karymbalis E, Skilodimou HD, Gaki-Papanastassiou K, Baltas EA (2016) Urban flood hazard assessment in the basin of Athens Metropolitan city, Greece. *Environ Earth Sci* 75(4):319
- Bathrellos GD, Skilodimou HD, Chousianitis K, Youssef AM, Pradhan B (2017) Suitability estimation for urban development using multi-hazard assessment map. *Sci Total Environ* 575:119–134
- Bogdanovic D, Nikolic D, Ilic I (2012) Mining Method Selection by Integrated AHP and PROMETHEE Method. *Anais da Academia Brasileira de Ciências* 84:219–233
- Cao C, Xu P, Wang Y, Chen J, Zheng L, Niu C (2016) Flash flood hazard susceptibility mapping using frequency ratio and statistical index methods in coalmine subsidence areas. *Sustainability* 8:948
- Cerdà A, Giménez-Morera A, Bodí MB (2009) Soil and water losses from new citrus orchards growing on sloped soils in the western Mediterranean basin. *Earth Surf Proc Land* 34:1822–1830
- Cerdà A, González-Pelayo O, Giménez-Morera A, Jordán A, Pereira P, Novara A, Brevik EC, Prosdociami M, Mahmoodabadi M, Keesstra S, García Orenes F, Ritsema C (2015) The use of barley straw residues to avoid high erosion and runoff rates on persimmon plantations in Eastern Spain under low frequency high magnitude simulated rainfall events. *Soil Res* 54(2):154–165
- Cerdà A, González-Pelayo O, Giménez-Morera A, Jordán A, Pereira P, Novara A, Brevik EC, Prosdociami M, Mahmoodabadi M, Keesstra S, Orenes FG, Ritsema CJ (2016) Use of barley straw residues to avoid high erosion and runoff rates on persimmon plantations in Eastern Spain under low frequency-high magnitude simulated rainfall events. *Soil Res* 54(2):154–165
- Cerdà A, Keesstra SD, Rodrigo-Comino J, Novara A, Pereira P, Brevik E, Jordán A (2017a) Runoff initiation, soil detachment and connectivity are enhanced as a consequence of vineyards plantations. *J Environ Manag* 202:268–275
- Cerdà A, Rodrigo-Comino J, Giménez-Morera A, Keesstra SD (2017b) An economic, perception and biophysical approach to the use of oat straw as mulch in Mediterranean rainfed agriculture land. *Ecol Eng* 108:162–171
- Chen W, Li W, Chai H, Hou E, Li X, Ding X (2016) GIS-based landslide susceptibility mapping using analytical hierarchy process (AHP) and certainty factor (CF) models for the Baozhong region of Baoji City, China. *Environ Earth Sci* 75:63
- Chitsaz N, Banihabib ME (2015) Comparison of different multi criteria decision-making models in prioritizing flood management alternatives. *Water Resour Manag* 29:2503–2525
- Conforti M, Aucelli PC, Robustelli G, Scarciglia F (2011) Geomorphology and GIS analysis for mapping gully erosion susceptibility in the Turbolo stream catchment (Northern Calabria, Italy). *Nat Hazard* 56:881–898
- Conoscenti C, Agnesi V, Angileri S, Cappadonia C, Rotigliano E, Ma'rkner M (2013) A GIS-based approach for gully erosion susceptibility modelling: a test in Sicily, Italy. *Environ Earth Sci* 70:1179–1195
- Conoscenti C, Angileri S, Cappadonia C, Rotigliano E, Agnesi V, Ma'rkner M (2014) Gully erosion susceptibility assessment by means of GIS-based logistic regression: a case of Sicily (Italy). *Geomorphology* 204(1):399–411
- Ding Q, Chen W, Hong H (2017) Application of frequency ratio, weights of evidence and evidential belief function models in landslide susceptibility mapping. *Geocarto Int* 32(6):619–639

- Dube F, Nhapi I, Murwira A, Gumindoga W, Goldin J, Mashauri DA (2014) Potential of weight of evidence modelling for gully erosion hazard assessment in Mbire District—Zimbabwe. *Phys Chem Earth* 67:145–152
- European Commission (EC): Communication from the Commission to the Council, the European Parliament, the European Economic and Social Committee and the Committee of the Regions (2006) Thematic Strategy for Soil Protection, COM 231 Final. Brussels
- Geology Survey of Iran (GSI) (1997) http://www.gsi.ir/Main/Lang_en/index.html
- Gómez-Gutiérrez A, Schnabel S, Felicísimo AM (2009) Modelling the occurrence of gullies in rangelands of southwest Spain. *Earth Surf Process Landf* 34:1894–1902
- Golestani G, Issazadeh L, Serajamani R (2014) Lithology effects on gully erosion in Ghoori chay Watershed using RS & GIS. *Int J Biosci* 4(2):71–76
- Gómez-Gutiérrez A, Conoscenti C, Angileri SE, Rotigliano E, Schnabel S (2015) Using topographical attributes to evaluate gully erosion proneness (susceptibility) in two mediterranean basins: advantages and limitations. *Nat Hazards* 79(1):291–314
- Griggs D, Stafford-Smith M, Gaffney O, Rockström J, Öhman MC, Shyamsundar P, Noble I (2013) Policy: sustainable development goals for people and planet. *Nature* 495(7441):305–307
- Guo-liang D, Yong-shuang Z, Javed I, Zhi-hua Y, Xin Y (2017) Landslide susceptibility mapping using an integrated model of information value method and logistic regression in the Bailongjiang watershed, Gansu Province, China. *J Mt Sci* 14(2):249–268
- Haghizadeh A, Siahkamari S, Haghiahi AH, Rahamti O (2017) Forecasting flood-prone areas using Shannon's entropy model. *J Earth Syst Sci* 126:39
- Hayas A, Vanwallegem T, Laguna A, Peña A, Giráldez JV (2017) Reconstructing long-term gully dynamics in Mediterranean agricultural areas. *Hydrol Earth Syst Sci* 21:235–249
- Hong H, Chen W, Xu C, Youssef A, Pradhan B, Bui D (2017) Rainfall-induced landslide susceptibility assessment at the Chongren area (China) using frequency ratio, certainty factor, and index of entropy. *Geocarto Int* 32(2):139–154
- Iranian Department of Water Resources Management (IDWRM) (2013) Weather and climate report. <http://www.thrw.ir/>. Accessed 25 Jun 2013
- Jaafari A, Najafi A, Pourghasemi HR, Rezaei J, Sattarian A (2014) GIS-based frequency ratio and index of entropy models for landslide susceptibility assessment in the Caspian forest, northern Iran. *Int J Environ Sci Technol* 11:909–926
- Jiuchun Y, Shuwen Z, Liping C, Fei L, Tianqi L, Yan G (2017) Gully erosion regionalization of black soil area in Northeastern China. *Chin Geogra* 27:78–87
- Keesstra SD, Bouma J, Wallinga J, Tittonell P, Smith P, Cerdà A, Montanarella L, Quinton JN, Pachepsky Y, van der Putten WH, Bardgett RD, Moolenaar S, Mol G, Jansen B, Fresco LO (2016) The significance of soils and soil science towards realization of the United Nations Sustainable Development Goals. *Soil* 2:111–128
- Keesstra S, Nunes J, Novara A, Finger D, Avelar D, Kalantari Z, Cerdà A (2018) The superior effect of nature based solutions in land management for enhancing ecosystem services. *Sci Total Environ* 610:997–1009
- Kim Y, Chung ES (2013) Assessing climate change vulnerability with group multi-criteria decision making approaches. *Climatic Chang* 121(2):301–315
- Kirchhoff M, Rodrigo Comino J, Seeger M, Ries JB (2017) Soil erosion in sloping vineyards under conventional and organic land use managements (Saar-Mosel valley, Germany). *Cuadernos de Investigación Geográfica* 43:119–140
- Kornejady A, Heidari K, Nakhavali M (2015) Assessment of landslide susceptibility, semi-quantitative risk and management in the Ilam dam basin, Ilam. *Iran Environ Resour Res* 3(1):85–109
- Kornejady A, Ownegh M, Bahremand A (2017) Landslide susceptibility assessment using maximum entropy model with two different data sampling methods. *Catena* 152:144–162
- Kuhnert PM, Henderson AK, Bartley R, Herr A (2010) Incorporating uncertainty in gully erosion calculations using the random forests modelling approach. *Environmetrics* 21:493–509
- Ligonja PJ, Shrestha RP (2015) Soil erosion assessment in kondoia eroded area in Tanzania using universal soil loss equation, geographic information systems and socioeconomic approach. *Land Degrad Dev* 26(4):367–379
- Lo CP, Yeung AKW (2002) Concepts and techniques of geographic information system. Pearson Education Inc., New Jersey
- Macharis C, Springael J, Brucker KD, Verbeke A (2004) PROMETHEE and AHP: the design of operational synergies in multicriteria analysis, strengthening PROMETHEE with ideas of AHP. *Eur J Oper Res* 153:307–317
- Manap MA, Nampak H, Pradhan B, Lee S, Sulaiman WNA, Ramli MF (2014) Application of probabilistic based frequency ratio model in groundwater potential mapping using remote sensing data and GIS. *Arab J Geosci* 7(2):711–724
- Märker M, Pelacani S, Schröder B (2011) A functional entity approach to predict soil erosion processes in a small Plio-Pleistocene Mediterranean catchment in Northern Chianti, Italy. *Geomorphology* 125(4):530–540
- Mekonnen M, Keesstra SD, Baartman JE, Stroosnijder L, Maroulis J (2017) Reducing sediment connectivity through man-made and natural sediment sinks in the minizir catchment, Northwest Ethiopia. *Land Degrad Dev* 28(2):708–717
- Moore ID, Burch GJ (1986) Physical basis of the length-slope factor in the Universal soil loss equation. *Soil Sci Soc Am J* 50:1294–1298
- Moore ID, Grayson RB, Ladson AR (1991) Digital terrain modeling: a review of hydrological, geomorphological, and biological applications. *Hydrol Process* 5:3–30
- Nefeslioglu HA, Duman TY, Durmaz S (2008) Landslide susceptibility mapping for a part of tectonic Kelkit Valley (Eastern Black Sea region of Turkey). *Geomorphology* 94(3):401–418
- Oh H, Lee S, Hong SM (2017) Landslide susceptibility assessment using frequency ratio technique with iterative random sampling. *J Sens* 1–21
- Papadakis M, Karimalis A (2017) Producing a landslide susceptibility map through the use of analytic hierarchical process in finikas watershed, North Peloponnese, Greece. *Am J Geogr Inf Syst* 6(1A):14–22
- Pawluszek K, Borkowski A (2017) Impact of DEM-derived factors and analytical hierarchy process on landslide susceptibility mapping in the region of Rożnow Lake, Poland. *Nat Hazards* 86:919–952
- Pourghasemi HR, Mohammady M, Pradhan B (2012) Landslide susceptibility mapping using index of entropy and conditional probability models in GIS: safarood basin, Iran. *CATENA* 97:71–84
- Pourghasemi HR, Pradhan B, Gokceoglu C, Moezzi KD (2013) A comparative assessment of prediction capabilities of Dempster-Shafer and Weights-of-evidence models in landslide susceptibility mapping using GIS. *Geo, Nat Haz Risk* 4(2):93–118
- Pourghasemi HR, Yousefi S, Kornejady A, Cerdà A (2017) Performance assessment of individual and ensemble data-mining techniques for gully erosion modeling. *Sci Total Environ* 609:764–775
- Rahmati O, Haghizadeh A, Pourghasemi HR, Noormohamadi F (2016) Gully erosion susceptibility mapping: the role of GIS based bivariate statistical models and their comparison. *Nat Hazards* 82:1231–1258
- Rahmati O, Tahmasebipour N, Haghizadeh A, Pourghasemi HR, Feizizadeh B (2017) Evaluating the influence of geo-environmental factors on gully erosion in a semi-arid region of Iran: An integrated framework. *Sci Total Environ* 579:913–927
- Razavizadeh S, Solaiman K, Massironi M, Kaviani A (2017) Mapping landslide susceptibility with frequency ratio, statistical index, and

- weights of evidence models: a case study in northern Iran. *Environ Earth Sci* 76:499
- Saaty TL (1980) *The analytic hierarchy process*. McGraw Hill, New York
- Saaty TL, Vargas GL (2001) *Models, methods, concepts, and applications of the analytic hierarchy process*. Kluwer Academic Publisher, Boston
- Süzen ML, Doyuran V (2004) A comparison of the GIS based landslide susceptibility assessment methods: multivariate versus bivariate. *Environ Geol* 45(5):665–679
- Svoray T, Michailov E, Cohen A, Rokah L, Sturm A (2012) Predicting gully initiation: comparing data mining techniques, analytical hierarchy processes and the topographic threshold. *Earth Surf Proc Land* 37:607–619
- Tahmassebpour N, Rahmati O, Noormohamadi F, Lee S (2016) Spatial analysis of groundwater potential using weights-of-evidence and evidential belief function models and remote sensing. *Arab J Geosci* 9:79
- USDA-SCS (1966) Procedure for determining rates of land damage, land depreciation, and volume of sediment produced by gully erosion. Technical Release No. 32. US GPO 1990-261-419:20727/SCS.US Government Printing Office, Washington, DC
- Vidal AL, Sahin E, Martelli N, Berhoune M, Bonan B (2010) Applying AHP to select drugs to be produced by anticipation in chemotherapy compounding unit. *J Exp Syst Appl*, Adelphi 37(2):1528–1534
- Wang Q, Li W (2017) A GIS-based comparative evaluation of analytical hierarchy process and frequency ratio models for landslide susceptibility mapping. *Phys Geogr* 38(4):318–337
- Wang Q, Li W, Chen W, Bai H (2015) GIS-based assessment of landslide susceptibility using certainty factor and index of entropy models for the Qianyang County of Baoji city, China. *J. Earth Syst. Sci* 124(7):1399–1415
- Water Resources Company of Semnan (WRCS) (2015) Precipitation and temperature reports. <http://www.Semnanrw>
- Wen F, Xin-sheng W, Yan-bo C, Bin Z (2017) Landslide susceptibility assessment using the certainty factor and analytic hierarchy process. *J Mt Sci* 14(5):906–925
- Wu Y, Li W, Wang Q, Liu Q, Yang D (2016) Landslide susceptibility assessment using frequency ratio, statistical index and certainty factor models for the Gangu County, China. *Arab J Geosci* 9:84
- Xie Z, Chen G, Meng X, Zhang Y, Qiao L, Tan L (2017) A comparative study of landslide susceptibility mapping using weight of evidence, logistic regression and support vector machine and evaluated by SBAS-InSAR monitoring: Zhouqu to Wudu segment in Bailong River Basin, China. *Environ Earth Sci* 76:313
- Yacov Y (2011) Harmonizing the omnipresence of MCDM in technology, society, and policy. Chapter 2
- Yilmaz C, Topal T, Süzen ML (2012) GIS-based landslide susceptibility mapping using bivariate statistical analysis in Devrek (Zonguldak-Turkey). *Environ Earth Sci* 65(7):2161–2178
- Zabihi M, Mirchooli F, Motevalli A, Darvishan AK, Pourghasemi HR, Zakeri MA, Sadighi F (2018) Spatial modelling of gully erosion in Mazandaran Province, northern Iran. *Catena* 161:1–13
- Zakerinejad R, Maerker M (2015) An integrated assessment of soil erosion dynamics with special emphasis on gully erosion in the Mazayjan basin, southwestern Iran. *Nat Hazards* 79:25–50
- Zhou C, Ge L, Dongchen E, Hsingchung C (2005) A case study of using external DEM in InSAR DEM generation. *Geo-spat Inform Sci* 8(1):14–18. <https://doi.org/10.1007/BF02826985>